

The Projected Changes in the Surface Energy Budget of the CMIP5 and EURO-CORDEX Models: Are We Heading toward Wetter Growing Seasons in Central Europe?

PETR SKALÁK^{a,b}, JAN MEITNER^{a,b}, MILAN FISCHER^{a,b}, MATĚJ ORSÁG^{a,b}, ALEXANDER GRAF^c,
MONIKA HLAVSOVÁ^{a,b} AND MIROSLAV TRNKA^{a,b}

^a *Global Change Research Institute, Brno, Czech Republic*

^b *Department of Agrosystems and Bioclimatology, Mendel University in Brno, Brno, Czech Republic*

^c *Forschungszentrum Jülich GmbH, Jülich, Germany*

(Manuscript received 22 January 2024, in final form 4 December 2024, accepted 30 December 2024)

ABSTRACT: We analyze the surface energy budget from four climate model ensembles and its future changes in the twenty-first century under the RCP8.5 or shared socioeconomic pathway (SSP) 5-8.5 scenario. High-resolution European domain of the Coordinated Regional Climate Downscaling Experiment (EURO-CORDEX) regional climate models (RCMs) and their driving CMIP5 global climate models (CMIP5-D) are first tested in central Europe against observational datasets. Evaluation reveals the added value of RCMs in terms of spatial variability and smaller biases. CMIP5-D are affected by the positive bias of global irradiance that propagates into other radiation and heat fluxes. There are strong differences in the projected surface energy budget components between RCMs and CMIP5-D. There is an increase in global irradiance for most of the year in CMIP5-D and other GCM ensembles that is translated into a year-round enhancement of the absorbed solar energy and balanced by higher latent heat flux, except in summer, when the sensible heat flux rises strongly. Together with strong warming and reduced precipitation in summer, this leads to warm, sunny, and dry conditions with reduced evapotranspiration and higher drought stress for vegetation. In the RCMs, the reduction in global irradiance dominates, and it is translated into a round-year reduction in the net balance of longwave radiation and stronger latent heat flux. The first months of the growing season show weaker warming associated with higher evapotranspiration and precipitation. In summer, precipitation drops and global irradiance and warming rise, but they fall behind the changes in the GCMs. Compared to GCMs, there are less visible signs of conditions leading to a reduction in evapotranspiration or a shortage of soil water in the RCMs in summer.


KEYWORDS: Europe; Climate change; Energy budget/balance; Climate models

1. Introduction

The future evolution of the climate and its impact on life on Earth is currently one of the biggest questions and challenges. The current knowledge about climate and its future development is regularly reviewed by assessment reports of the Intergovernmental Panel on Climate Change (IPCC). The most recent Sixth Assessment Report of IPCC Working Group 1 (IPCC 2021) is also accompanied by the new Interactive Atlas of Climate Change (Gutiérrez et al. 2023), which provides deeper insight into expected climate change at the regional level. The climate projections summarized in the sixth IPCC report are based on simulations of a large ensemble of global climate models (GCMs) from phase 6 of the Coupled Model Intercomparison Project (CMIP6) (Eyring et al. 2016; O'Neill et al. 2016) and their comparison with a previous generation of climate models from the CMIP5 ensemble (Taylor et al. 2012). The Interactive Atlas of Climate Change also includes projections that are based on simulations of regional climate models (RCMs) from the global Coordinated Regional Climate Downscaling

Experiment (CORDEX) initiative (Giorgi et al. 2009). The CORDEX projections presented in the IPCC Atlas were created by dynamical downscaling (Wilby and Wigley 1997) of the CMIP5 GCMs using the state-of-the-art RCMs.

A significant advantage of RCM projections compared to those based on GCMs is their better spatial resolution, which may reach up to 12 km in some regions (e.g., Europe). In contrast, the spatial resolution of the vast majority of CMIP6 GCMs remains at the level of 100–300 km. Many important mesoscale processes in the climate system, which shape the climate at the regional level, are thus not fully resolved in GCMs but may be well captured in RCMs. Therefore, there is a continuing effort in the scientific community to bring RCM simulations toward finer spatial scales of kilometers with full resolution of atmospheric convection (Prein et al. 2017; Kendon et al. 2021; Lucas-Picher et al. 2021). Additionally, there is an effort to increase the complexity of RCMs and include further components of the climate system, similar to CMIP Earth system models (Giorgi 2019). As noted by Giorgi (2019), RCM projections are the preferred choice for the analysis of climate change and its impacts on the subcontinental scale corresponding to, e.g., individual countries or even smaller administrative regions. RCMs thus represent the beginning of the information and processing chain that ends with proposals of targeted adaptation measures, political decisions, and the related financial costs.

 Denotes content that is immediately available upon publication as open access.

Corresponding author: Petr Skalák, skalak.p@czechglobe.cz

DOI: 10.1175/JHM-D-24-0017.1

© 2025 American Meteorological Society. This published article is licensed under the terms of a Creative Commons Attribution 4.0 International (CC BY 4.0) License



Central Europe is a transition area between two important poles of observed and projected climate change in Europe: warmer and wetter Scandinavia and warmer but drier Mediterranean (Coppola et al. 2021; Gutiérrez et al. 2023). The uncertainty in the projected changes in the central European climate will further increase if different model ensembles (GCM vs RCM) are considered (Bartók et al. 2017; Fernández et al. 2019; Boé et al. 2020; Coppola et al. 2021). However, significant differences between GCMs and RCMs also appear when both model ensembles are compared with observed trends or long-term mean values of climate variables in the second half of the twentieth century (Enriquez-Alonso et al. 2017; Bartók et al. 2017).

Enriquez-Alonso et al. (2017) found that RCMs are unable to capture the observed decadal trend in total cloudiness in the Mediterranean area, while their driving GCMs can reproduce it and show a statistically significant decreasing trend corresponding to observations. Similarly, Bartók et al. (2017) described significant differences in the projection of global radiation over Europe in the twenty-first century among the European domain of the CORDEX (EURO-CORDEX) RCMs and their driving GCMs. They also detected different trends of global radiation in both model ensembles when compared with observations and attributed these differences to time-invariant aerosol concentrations in RCMs. The latter can also partly affect air temperature trends over Europe simulated by RCMs driven by reanalysis. As noted by Nabat et al. (2014), the air temperature trends in this type of RCM simulation do not correspond to observations.

The most prominent difference between RCM and GCM projections in Europe is a reduction in summer warming by RCMs (Sørland et al. 2018). It is also associated with the smaller decrease in precipitation and smaller increase in global radiation in RCMs compared to GCMs (Boé et al. 2020). However, the projected seasonal means or various climate indices based on air temperature or precipitation may also differ among EURO-CORDEX RCMs, their driving CMIP5 GCMs, or newer CMIP6 GCMs in other seasons (Fernández et al. 2019; Coppola et al. 2021), although less significantly than in the summer.

Several mechanisms have been proposed to explain disagreements among GCM and RCM projections of air temperature, precipitation, or global radiation in Europe during the twenty-first century. The absence of time-varying anthropogenic aerosols in most RCM simulations plays a major role in the differences in solar radiation changes (Boé et al. 2020; Taranu et al. 2023). Boé et al. (2020) also noted that RCMs simulate a much larger increase in evaporation over the Mediterranean Sea. This could likely affect the relative humidity changes over the continent, leading to a smaller reduction in cloud cover, precipitation, and finally evapotranspiration and thus a smaller increase in air temperature. Nevertheless, the causes of these evaporation changes over the sea remain unclear. Schwingshackl et al. (2019) proposed that RCM projections may also underestimate future warming due to missing plant physiological CO₂ responses. This process is captured by most GCMs, but plants do not reduce their transpiration under elevated CO₂ conditions in RCMs, which leads to

lower surface temperatures, especially during temperature extremes. However, plant physiology seems to be unlikely to act as the dominant factor in the detected GCM/RCM discrepancies according to Taranu et al. (2023). Fernández et al. (2019) noted that the overall design of the EURO-CORDEX ensemble with only a few favored GCMs selected for downscaling and a larger share of some RCMs in the final ensemble may affect the final climate change signal of the RCM ensemble. Similarly, Taranu et al. (2023) have shown that inconsistencies in the projected climate change may be limited when GCMs and RCMs share similar settings (same resolution, same physics, same forcings).

The main goal of this study is to analyze differences in projections of individual components of the surface energy budget (Earth's surface radiation and heat balance) provided by EURO-CORDEX RCMs and their driving CMIP5 GCMs across the central European domain. Special emphasis is placed on the projected changes in latent and sensible heat fluxes. Both turbulent heat fluxes may act as indicators of bioclimatic conditions, and their changes reflect the combined effect of air temperature, precipitation, or global radiation on vegetation and ecosystems. While the changes in the sensible heat flux affect the temperatures, including the extremes, the boundary layer depth, and consequently the cloud formation (Katul et al. 2012), the latent heat flux is closely connected to water vapor transport, which represents a major part of the hydrological cycle across central Europe. Another aim of the study is to evaluate components of the surface energy budget simulated by EURO-CORDEX RCMs and their driving CMIP5 GCMs in the past climate. Unlike temperature or precipitation, the surface energy budget components are less often a subject of validation. This is to identify potential shortcomings of climate models that could affect the interpretation of future projections.

2. Data and methods

We analyze the components of Earth's surface energy budget available from climate models with the focus on the summer half year (April–September). The selected period roughly corresponds to the growing season in the study area (central Europe). Individual radiation and heat fluxes are considered as long-term monthly averages over a period of 25 years (1981–2005 in the past and 2076–2100 in the future).

The selected study area (further referred as central Europe) is defined as the rectangle between 9°–21° of the eastern longitude and 47°–54° of northern latitude. The area is approximately centered over the Czech Republic but covers a larger area including parts of Germany, Poland, Slovakia, Hungary, Austria, and Switzerland. It also includes part of the eastern ridge of the Alps (see Fig. 1). The region is characterized by a complex landscape with various vegetation types (mainly agricultural land, pastures, and mixed forests) and altitudes mostly up to 1000 m. It is an intensively used agricultural landscape and a source of water for several major European rivers. The territory of all abovementioned countries including their parts outside of the defined study area is considered as a wider area of central Europe.

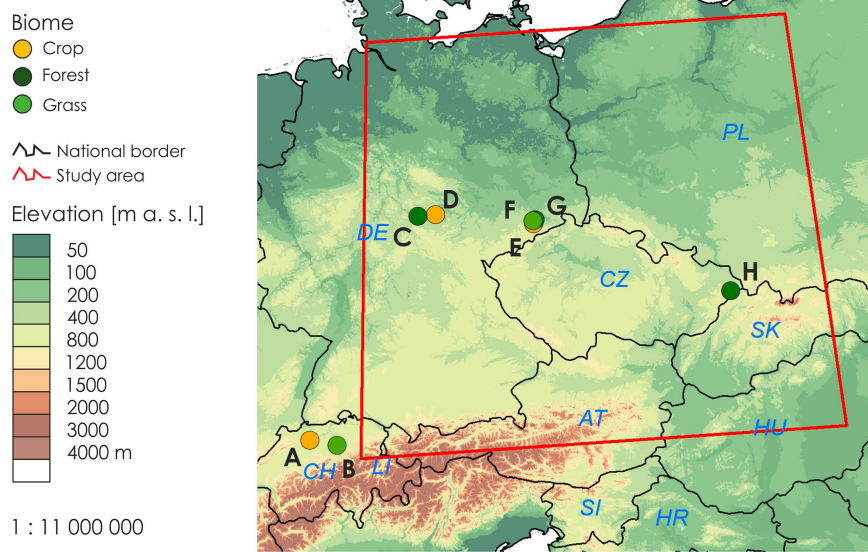


FIG. 1. Study area in Europe with highlighted locations of FLUXNET sites used for evaluation of the climate models and ERA5-Land reanalysis. More detailed information about the FLUXNET sites can be found in [Table A1](#) in the [appendix](#).

a. Climate variables

The simplified Earth's surface energy budget can be written as follows:

$$S_d - S_u = L_u - L_d + H + LE + G, \quad (1)$$

where S_d is the incoming shortwave solar radiation (also called global irradiance), S_u is the solar radiation reflected from Earth's surface, L_u is the outgoing longwave radiation from Earth's surface, L_d is the incoming longwave radiation from the atmosphere, H is the sensible heat flux, LE is the latent heat flux (positive when energy is transported from the surface to the atmosphere), and G is the heat flux into soil. Note that according to the sign convention used, positive values of S_d and L_d represent a gain of energy on Earth's surface, while positive values of S_u , L_u , H , and LE correspond to a loss of energy on Earth's surface. The vertical heat flux from/to soil is not used in the study, as it is not commonly available in climate model data. The terms on the left-hand side of Eq. (1), S_d and S_u , represent the net balance of shortwave (NetSW) radiation:

$$\text{NetSW} = S_d - S_u. \quad (2)$$

Similarly, the first two terms on the right-hand side of Eq. (1), L_u and L_d , represent the net balance of longwave (NetLW) radiation:

$$\text{NetLW} = L_u - L_d. \quad (3)$$

The difference of both balances, NetSW and NetLW, forms the net radiation (NetRAD) balance of Earth's surface:

$$\text{NetRAD} = \text{NetSW} - \text{NetLW}. \quad (4)$$

To study the relative contributions of the turbulent energy fluxes (H and LE) to Earth's surface energy budget, we use the evaporative fraction (EF), defined as follows:

$$EF = \frac{LE}{H + LE}. \quad (5)$$

b. Climate models

We consider four sets of climate models: one set of RCMs, two sets of CMIP5 GCMs, and one set of CMIP6 GCMs. The RCM data came from the European part of the CORDEX global experiment (EURO-CORDEX) and have a spatial resolution of 0.44° on the RCM native rotated grid (corresponding to ~ 50 -km grid spacing). Unlike previous studies ([Stagehuis et al. 2013](#); [Knist et al. 2017](#)), we exclusively work with simulations driven by CMIP5 GCMs and not with reanalysis, as our goal is to analyze the climate change signal and understand how GCM-RCM modeling pairs (as a tool to simulate the future) are successful in capturing the climate of the recent past. We also do not use the more detailed EURO-CORDEX simulations with a 0.11° resolution, as the potential added value of RCMs compared to GCMs should already be apparent in the coarser resolution of 0.44° . Our selection should also suppress possible errors in RCM simulations that stem from a gap in the horizontal resolution between RCM and its driving GCM data or from limitations of RCM physical parameterizations under very high resolution.

In total, we considered nine RCM simulations ([Table 1](#)), where all the necessary surface energy budget data were available at the Earth System Grid Federation data nodes at the time when this study was initiated. There are four different RCMs in the selected EURO-CORDEX ensemble; however, their share is not equal. While two RCMs (CLM4.8.17 and HIRHAM5) are represented by only one simulation each, the RCA4 simulation driven by various GCMs has the largest share (five out of nine simulations).

The second model ensemble used in this study is composed of five GCMs that serve as a source of lateral boundary conditions

TABLE 1. Summary of EURO-CORDEX RCMs and their CMIP5-D.

RCM name	CMIP5-D				
	CNRM-CM5	EC-EARTH	HADGEM2-ES	IPSL-CM5A-MR	MPI-ESM-LR
CLM4.8.17					X
HIRHAM5		X			
RACMO22E		X	X		
RCA4	X	X	X	X	X

for EURO-CORDEX RCMs. All driving GCMs (hereinafter CMIP5-D) are mentioned in Table 1 and listed with more details in Table 2.

Climate projections of RCMs and CMIP5-D are also compared to projections of larger model ensembles. First, it is a 15-member ensemble (further referred to as CMIP5 ensemble) composed of five CMIP5-D and 10 additional GCMs from phase 5 of CMIP. Second, it is a group of 17 GCMs from phase 6 of CMIP. All models from both larger ensembles are listed in Table 2. There are two reasons to include additional GCMs into the analysis:

- 1) to understand how CMIP5-D projections, based on five GCMs only, are consistent with the mean climate change signal of the larger ensemble of CMIP5 models and

- 2) to see how RCM and CMIP5-D projections representing the previous generation of climate models are related to the climate change signal derived from the latest generation of CMIP6 GCMs.

For all sets of climate models, we calculated an ensemble mean as a simple arithmetic average across all ensemble members. Due to the absence of outgoing shortwave and longwave radiation (S_u and L_u) data in the EC-EARTH model, the CMIP5-D ensemble mean for all radiation balances (NetSW, NetLW, and NetRAD) was based on only four GCMs. When plotting the GCM ensemble mean on a map, the data of individual GCMs were first interpolated to the common grid of 1.5° resolution in longitude and latitude, and

TABLE 2. Summary of CMIP5 and CMIP6 GCMs.

Ensemble designation		No.	GCM name	Ensemble member	Horizontal resolution, lon × lat (°)
CMIP5	CMIP5-D	1	CNRM-CM5	r1i1p1	1.41 × 1.41
		2	EC-EARTH	r12i1p1	1.13 × 1.12
		3	HadGEM2-ES	r1i1p1	1.88 × 1.25
		4	IPSL-CM5A-MR	r1i1p1	2.50 × 1.27
		5	MPI-ESM-LR	r1i1p1	1.88 × 1.87
		6	BCC-CSM1-1	r1i1p1	2.81 × 2.79
		7	CESM1-BGC	r1i1p1	1.25 × 0.94
		8	CESM1-CAM5	r1i1p1	1.25 × 0.94
		9	CMCC-CESM	r1i1p1	3.75 × 3.71
		10	CMCC-CMS	r1i1p1	1.88 × 1.86
		11	GFDL-CM3	r1i1p1	2.50 × 2.00
		12	GFDL-ESM2G	r1i1p1	2.50 × 1.52
		13	INM-CM4	r1i1p1	2.00 × 1.50
		14	MRI-ESM1	r1i1p1	1.13 × 1.11
		15	NorESM1-M	r1i1p1	2.50 × 1.90
CMIP6	—	1	AWI-CM-1-1-MR	r1i1plf1	0.94 × 0.94
		2	BCC-CSM2-MR	r1i1plf1	1.13 × 1.12
		3	CESM2	r4i1plf1	1.25 × 0.94
		4	CMCC-CM2-SR5	r1i1plf1	1.25 × 0.94
		5	CMCC-ESM2	r1i1plf1	1.25 × 0.94
		6	CNRM-CM6-1-HR	r1i1plf2	0.50 × 0.50
		7	GFDL-CM4	r1i1plf1	1.25 × 1.00
		8	GFDL-ESM4	r1i1plf1	1.25 × 1.00
		9	EC-EARTH3	r1i1plf1	0.70 × 0.70
		10	EC-EARTH3-CC	r1i1plf1	0.70 × 0.70
		11	EC-EARTH3-VEG	r1i1plf1	0.70 × 0.70
		12	HadGEM3-GC31-MM	r1i1plf3	0.83 × 0.56
		13	INM-CM5-0	r1i1plf1	2.00 × 1.50
		14	MPI-ESM1-2-HR	r1i1plf1	0.94 × 0.94
		15	MRI-ESM2-0	r1i1plf1	1.13 × 1.12
		16	NorESM2-MM	r1i1plf1	1.25 × 0.94
		17	TaiESM1	r1i1plf1	1.25 × 0.94

then, the ensemble mean map was calculated. Interpolation can be skipped when plotting maps for RCMs, as all models share the same grid in rotated geographic coordinates.

The projected changes in the surface energy balance were analyzed for the last quarter of the twenty-first century (2076–2100) and compared with the historical period 1981–2005. We used climate model simulations following the representative concentration pathway (RCP) scenario RCP8.5 in case of RCMs and CMIP5 GCMs and the shared socioeconomic pathway (SSP) scenario SSP5-8.5 for CMIP6 GCMs. The selected scenarios expect a continuing increase in greenhouse gas concentrations toward the end of the twenty-first century. The results of climate model simulations based on the RCP8.5 and SSP5-8.5 scenarios are thus expected to deliver the most significant changes in climate parameters compared to the current conditions.

To evaluate the significance of the results, we consider the projected ensemble mean changes significant only if they exceed the standard deviation calculated from changes of individual ensemble members.

c. Observational data

To evaluate the performance of climate models in the recent past (1981–2005), we used the European Centre for Medium-Range Weather Forecasts (ECMWF) ERA5-Land (ERA5L) reanalysis (Muñoz-Sabater et al. 2021) as the main validation dataset representing the observational data. ERA5-Land was created by interpolation of the main reanalysis ERA5 (Hersbach et al. 2017) into a finer spatial grid with a resolution of 0.1° in latitude and longitude. The validation was focused on a comparison of long-term monthly means of individual surface energy fluxes spatially averaged over the whole study area and their temporal course over the period from April to September.

To validate the global irradiance, we used two additional observational datasets: the E-OBS dataset of gridded station observation version 22e (Cornes et al. 2018) and the Surface Solar Radiation Dataset–Heliosat, edition 2.1 (SARAH-2), dataset (Pfeifroth et al. 2019) created within the Climate Satellite Application Facility of EUMETSAT.

The E-OBS dataset is based on the interpolated daily global irradiance data (directly measured or calculated from sunshine duration measurements) stored in the European Climate Assessment and Dataset (ECA&D) database and originally coming from station networks of national weather services and other data providers. Similar to ERA5-Land, E-OBS data are available in a regular grid with a mesh size of 0.1° in latitude and longitude.

SARAH-2 global irradiance data were derived from satellite observations and offer a higher spatial resolution of 0.05° in latitude and longitude. However, the first data were available as late as 1983, i.e., 2 years later than that in the ERA5-Land, E-OBS, or climate models.

Finally, we used measurements of surface energy balance components from selected stations of the flux network (FLUXNET) in central Europe. The data from FLUXNET sites cover the period 2001–18; however, availability may

differ among stations (Table A1 in the appendix). FLUXNET records were used here to illustrate surface turbulent heat fluxes behavior in different biomes typical for central Europe and to compare with climate model data.

d. Evaluation procedure

Mean bias and spatial correlations over the study area were used as two metrics to evaluate the performance of climate models by comparison with ERA5-Land reanalysis in the period 1981–2005. All data were transferred to the common regular grid of 1.5° resolution in longitude and latitude, and then, both metrics were calculated. RCMs were first interpolated to the regular grid of 0.5° resolution in longitude and latitude and then upsampled by spatial averaging in the matrix of nine grid points. As ERA5-Land comes on the regular 0.1° grid, it was upsampled by spatial averaging in the matrix of 225 grid points. GCMs were transferred from their native grids to the 1.5° grid by interpolation only.

3. Results

a. Evaluation in past climate conditions

The aim of this section is to analyze the performance of RCMs and their driving GCMs by comparison with ERA5-Land reanalysis in the period 1981–2005.

1) RADIATION FLUXES

The annual course of global irradiance, NetSW, and NetLW over the study area shows very good agreement among RCMs and ERA5-Land reanalysis (Figs. 2a–c). In summer, global irradiance and NetSW is slightly higher in RCMs (up to $+9 \text{ W m}^{-2}$ or $\sim +5\%$), but when other validation datasets (E-OBS and SARAH-2) are considered, there is good agreement among these datasets and RCMs, better than in the case of ERA5-Land. NetLW in RCMs is underestimated during the entire growing season (Fig. 2c), the most significantly in spring (down to -7 W m^{-2} or $\sim -10\%$). Spatial correlations of global irradiance and NetSW (Table 3) are higher than 0.8, sometimes even over 0.9, with only one exception (NetSW in May). On the other hand, NetLW correlations are lower in RCMs, ranging from 0.54 in May to 0.91 in September. When the RCM data are checked visually on its native grid, there is a clear signal of global irradiance reduction in the mountains, e.g., over the Carpathians or eastern Alps, in summer that is related to the annual course of convection and cloudiness in the region (Fig. A1 in the appendix). The summer reduction in global irradiance is also clearly visible in the SARAH-2 satellite data but not evident in the E-OBS and ERA5-Land data.

In the case of CMIP5-D, spatial correlations of radiation fluxes are very low (under 0.5), especially in summer months (Table 3). From April to July, spatial correlations of NetLW are even higher than for global irradiance or NetSW, an attribute that is not present in RCMs. However, the main feature of CMIP5-D is the positive bias of all radiation fluxes from May to September (Figs. 2a–c or Table 3). In June and July, global irradiance and NetSW are overestimated by

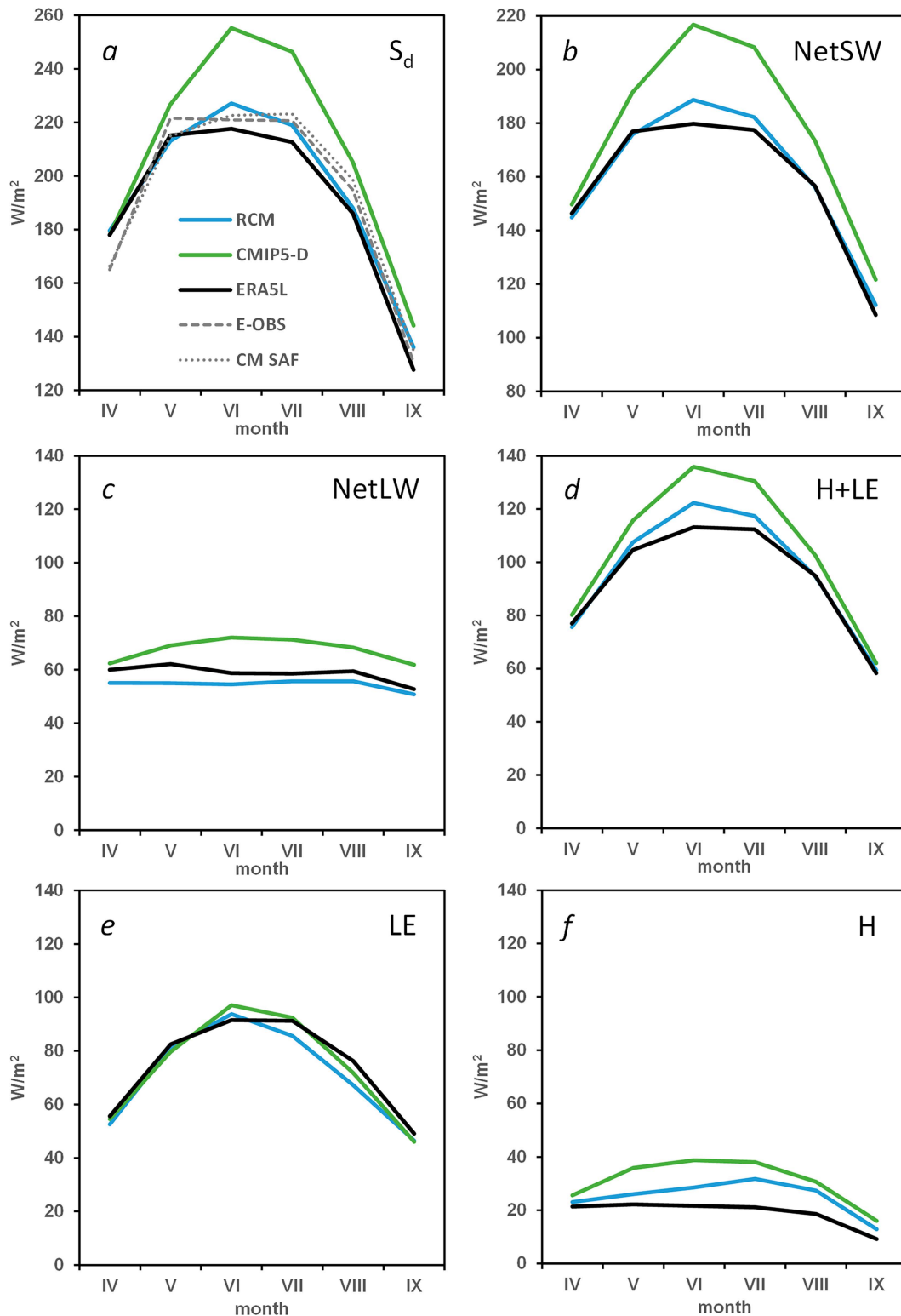


FIG. 2. Seasonal course of selected components of the surface energy budget (W m^{-2}) over central Europe from April (IV) to September (IX) as simulated by EURO-CORDEX RCMs, their CMIP5-D, and ERA5L: (a) global irradiance, (b) NetSW, (c) NetLW, (d) NetRAD, (e) LE, and (f) H . For global irradiance other two validation datasets, E-OBS and CM SAF SARA-H2, are also displayed.

TABLE 3. Mean bias and spatial correlations of selected radiation and heat fluxes in EURO-CORDEX RCMs and their CMIP5-D compared to ERA5L in central Europe from April (IV) to September (IX) in the period 1981–2005.

Parameter	Model ensemble	Mean bias (W m^{-2})						Spatial correlation (–)					
		IV	V	VI	VII	VIII	IX	IV	V	VI	VII	VIII	IX
S_d	CMIP5-D	0	12	38	34	19	17	0.52	0.27	–0.09	0.36	0.65	0.85
	RCM	2	–2	9	6	2	8	0.93	0.81	0.87	0.80	0.93	0.95
NetSW	CMIP5-D	3	15	37	31	17	13	0.45	0.48	–0.09	0.32	0.60	0.82
	RCM	–2	–1	9	5	0	4	0.87	0.65	0.83	0.80	0.93	0.95
NetLW	CMIP5-D	2	7	13	13	9	9	0.58	0.67	0.24	0.38	0.54	0.43
	RCM	–5	–7	–4	–3	–4	–2	0.78	0.54	0.74	0.71	0.69	0.91
$H + LE$	CMIP5-D	3	11	23	18	8	4	0.51	–0.10	–0.03	0.16	0.80	0.82
	RCM	–1	3	9	5	0	1	0.86	0.55	0.64	0.69	0.89	0.93
LE	CMIP5-D	–1	–3	6	1	–4	–3	0.17	0.12	0.22	0.30	0.57	0.70
	RCM	–3	–1	2	–6	–9	–3	0.76	0.77	0.16	–0.01	0.05	0.24
H	CMIP5-D	4	14	17	17	12	7	0.07	–0.33	–0.18	–0.14	–0.01	0.38
	RCM	2	4	7	11	9	4	0.24	0.05	–0.05	0.11	0.55	0.79

approximately 35 W m^{-2} and NetLW on 13 W m^{-2} or ca +20% in relative comparison.

2) TURBULENT HEAT FLUXES

The monthly LE of both model ensembles is in excellent agreement with ERA5-Land across the entire growing season (Fig. 2e). Although both ensembles slightly overestimate LE in June and underestimate LE in August, the differences are small, only a few watts per square meter (Table 3). Spatial correlations in RCMs are very low except for spring and generally lower than for radiation fluxes. When the RCM data are checked visually on its native grid, LE is relatively suppressed in RCMs over central European lowlands, while it remains high in ERA5-Land in summer (Fig. A2 in the appendix).

Compared to ERA5-Land, the monthly H is overestimated by CMIP5-D across the entire growing season and by RCMs mostly in summer (Fig. 2f). In CMIP5-D, the maximum differences reach $+17 \text{ W m}^{-2}$ (or $\sim +80\%$) in June and July (Table 3). In RCMs, the differences are smaller, between $+7$ and $+11 \text{ W m}^{-2}$ (or $\sim +50\%$). The overestimation of H in CMIP5-D is associated with compensation for the positive biases in global irradiance and NetSW, as shown in Figs. 2a and 2b. However, the enhancement of H itself is not the only mechanism to compensate for the relatively large bias of NetSW. As already mentioned, there is also stronger energy loss by longwave radiation in CMIP5-D, as is apparent from a positive bias of NetLW (see Fig. 2c).

In RCMs, the enhanced global irradiance and NetSW in June and July (up to $+9 \text{ W m}^{-2}$) compared to ERA5-Land are fully translated into an increased sum of both turbulent fluxes, $H + LE$ (Table 3). As the energy loss via NetLW is reduced in RCMs in June and July (Fig. 2c or Table 3), part of the energy is perhaps accumulated in the region via the heat flux into soil or transported horizontally by other mechanisms.

3) EVAPORATIVE FRACTION

Monthly values of the EF in CMIP5-D and ERA5-Land show a gradual increase during the entire growing season that

corresponds to the increasing share of LE in the net turbulent heat flux (Fig. 3). In absolute terms, however, the H monthly values are significantly larger in CMIP5-D, thus leading to an EF of approximately 0.7, while in ERA5-Land, the EF is higher, around 0.8. In RCMs, the EF values are close to ERA5-Land until June, but then they drop to 0.72 as the role of H grows, while LE declines in RCMs (Fig. 3).

b. Climate change projections

The aim of this section is to analyze the future changes of the surface energy budget components in EURO-CORDEX RCMs and their CMIP5-D and put those changes into a broader perspective of the projections from the larger ensembles of

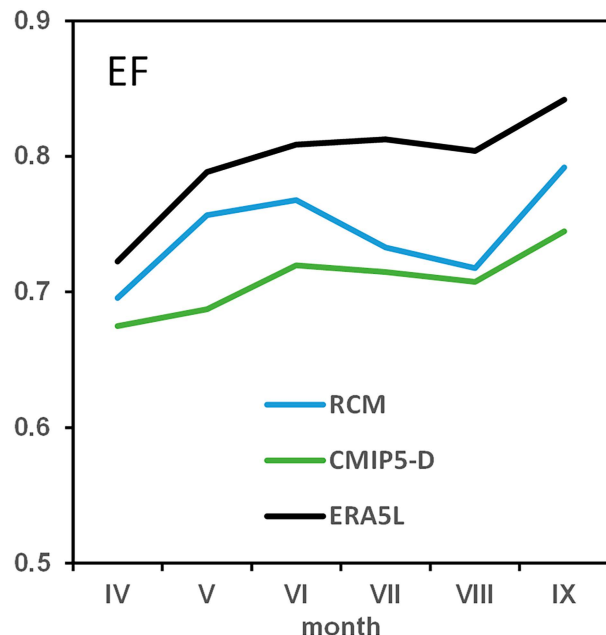


FIG. 3. Seasonal course of the EF in central Europe from April (IV) to September (IX) as simulated by EURO-CORDEX RCMs, their CMIP5-D, and ERA5L in the period 1981–2005.

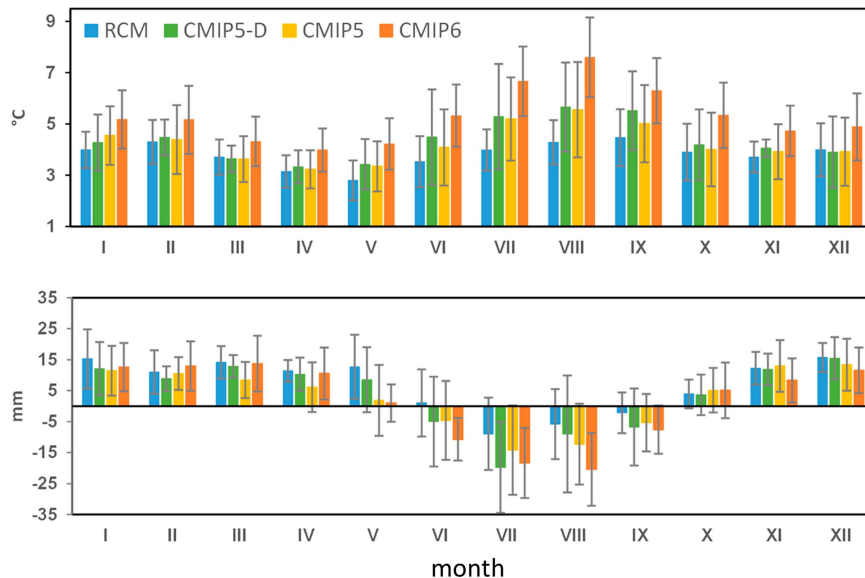


FIG. 4. Projected changes of (top) monthly air temperature and (bottom) precipitation in central Europe in the last quarter of the twenty-first century according to the RCP8.5 or SSP5-8.5 scenarios in EURO-CORDEX RCMs, their CMIP5-D, and other two larger ensembles of CMIP5 and CMIP6 GCMs. Whiskers indicate standard deviation of the ensemble mean changes.

CMIP5 and CMIP6 models. The RCP8.5 scenario is considered for RCMs and both ensembles of CMIP5 models, while the SSP5-8.5 scenario is taken for CMIP6 GCMs.

1) AIR TEMPERATURE

All model ensembles expect significant warming toward the end of the twenty-first century. The annual mean temperature should increase by $+4.4^{\circ}\text{C}$ according to CMIP5-D or by slightly less ($+3.8^{\circ}\text{C}$) according to RCMs. Warming is strongest in the second half of the growing season (July–September) and varies from $+4.0^{\circ}$ to 4.5°C in RCMs or from $+5.3^{\circ}$ to 5.7°C in CMIP5-D (Fig. 4, top). For most of the year (mainly outside the growing season), the differences between warming levels in RCMs and CMIP5-D are small: only a few tenths of a degree Celsius (Fig. 4, top). However, from June to September, the differences between both ensembles are bigger, from 1° to 1.4°C . When the larger CMIP5 ensemble is considered, the warming signal is usually close to CMIP5-D. In CMIP6, model's warming is stronger than in any other ensemble, as the new generation of CMIP6 GCMs show greater climate sensitivity than their CMIP5 counterparts (Meehl et al. 2020; Zelinka et al. 2020), and their scenario forcing, SSP5-8.5, is also not identical to RCP8.5. However, the main pattern of air temperature changes across the growing season remains the same.

2) PRECIPITATION

There are two main features in the projected precipitation changes in all model ensembles (Fig. 4, bottom). First, a reduction in precipitation from July to September (CMIP5-D: from -7 to -20 mm month^{-1} or -35 mm in total; RCMs: from -2 to -9 mm month^{-1} or -17 mm in total) that in the case of all GCM ensembles is present already in June (e.g.,

CMIP5-D: -5 mm month^{-1}). Second, there is an increase in precipitation from October to May (CMIP5-D: from $+4$ to $+15\text{ mm month}^{-1}$ or $+84\text{ mm}$ in total; RCMs: from $+1$ to $+16\text{ mm month}^{-1}$ or $+97\text{ mm}$ in total). A combination of both effects leads to higher annual precipitation sums of $+43\text{ mm}$ (or $+5\%$) in CMIP5-D and $+80\text{ mm}$ (or $+10\%$) in RCMs. There is a good agreement among all models on the higher monthly precipitation from November to April as indicated by ensemble standard deviations smaller than mean changes (Fig. 4, bottom). The reduction of precipitation in the second half of the growing season is less certain. For RCMs, after a significant increase in precipitation in April and May, changes of precipitation from June to September are insignificant. For CMIP5-D and CMIP5 models, all monthly changes from May to September are insignificant except for July. For CMIP6, however, the precipitation decrease from June to September is stronger than in any other ensemble and significant.

3) GLOBAL IRRADIANCE

The projected changes in global irradiance at the end of the twenty-first century differ a lot between RCMs and other GCM ensembles.

In CMIP5-D, global irradiance rises during the entire growing season and October (significantly except for April and May), in July by $+23\text{ W m}^{-2}$, and in August by $+21\text{ W m}^{-2}$ ($+10\%$ in both months) (Fig. 5a). In other months, the changes in global irradiance are small (a few W m^{-2}) and mainly negative (the most in March: -3.2 W m^{-2}). From April to June, the largest enhancement of global irradiance is detected in the southeastern part of central Europe, while from July to September, it is in the southwest (Fig. 6). In

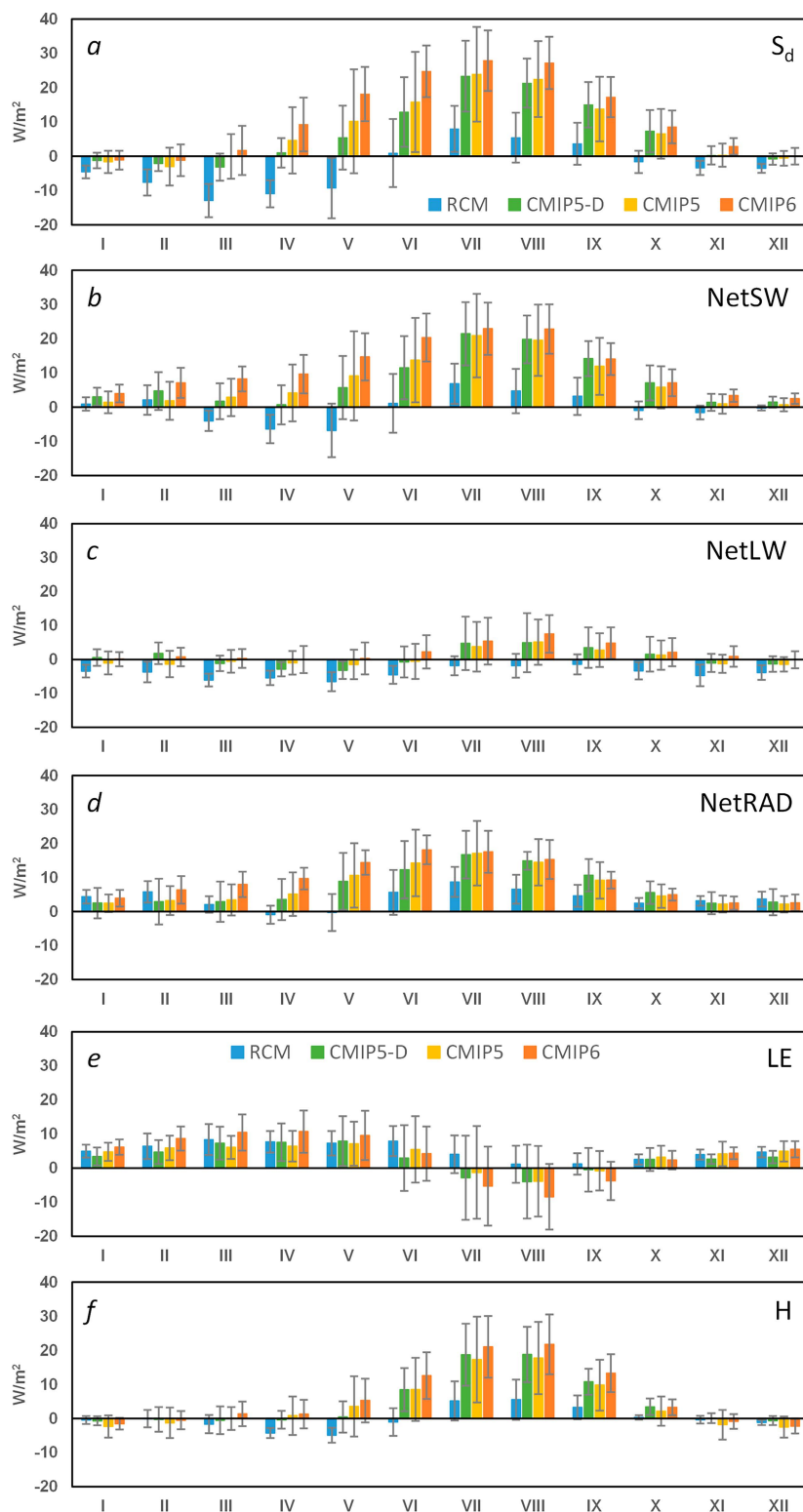


FIG. 5. Projected changes of (a) monthly global irradiance, (b) NetSW, (c) NetLW, (d) NetRAD, (e) LE, and (f) H in central Europe in the last quarter of the twenty-first century according to the RCP8.5 scenario or SSP5-8.5 scenarios in EURO-CORDEX RCMs, their CMIP5-D, and other two larger ensembles of CMIP5 and CMIP6 GCMs. Whiskers indicate standard deviation of the ensemble mean changes.

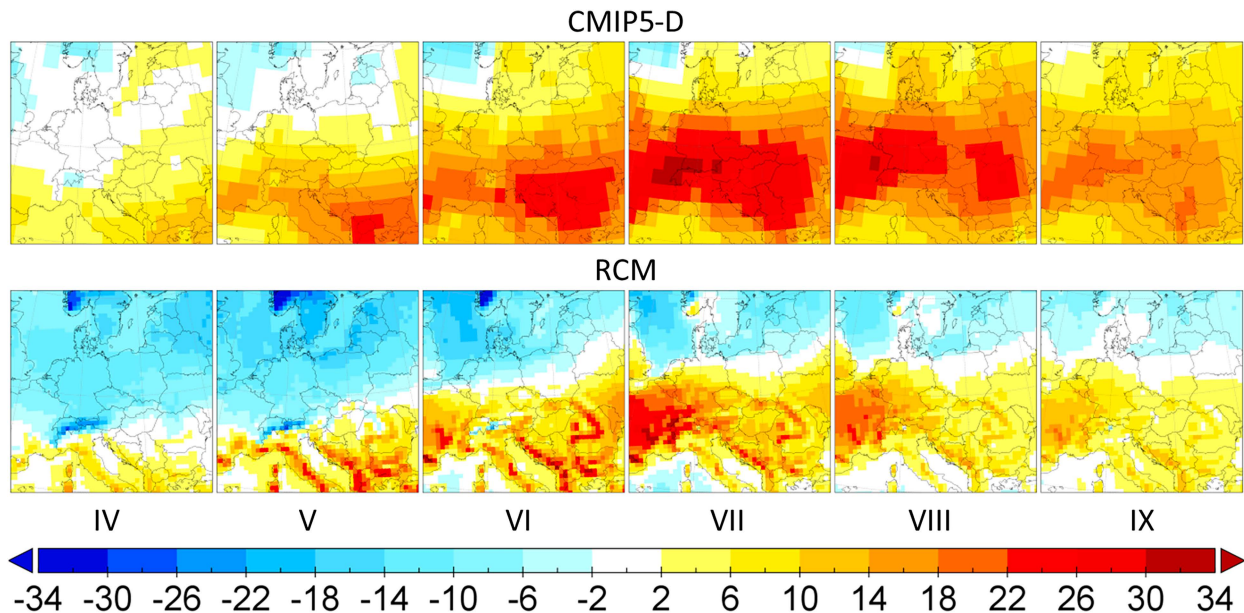


FIG. 6. Changes of global irradiance (W m^{-2}) from April (IV) to September (IX) in 2076–2100 compared to 1981–2005 projected by EURO-CORDEX RCMs and CMIP5-D GCMs.

other GCM ensembles, the main pattern of the projected changes is close to CMIP5-D. CMIP6 changes of global irradiance in the growing season are bigger than those of CMIP5-D and always significant.

In RCMs, we may also note an increase in global irradiance from July to September (maximum $+8.0 \text{ W m}^{-2}$ or $+4\%$ in July); however, changes are 3 or even 4 times smaller than those in GCM ensembles, insignificant except for July (Fig. 5a) and associated with the southwestern part of central Europe (Fig. 6). Moreover, global irradiance is suppressed in practically all other months, mainly in winter (up to -11% in relative terms) and in spring (March: -12.9 W m^{-2} , i.e., -10% ; April: 11.0 W m^{-2} , i.e., -6%). Strong reduction of global irradiance in spring is a distinct feature of RCMs that is not present in any of GCM ensembles.

4) OTHER RADIATION FLUXES

The future changes of NetSW in all model ensembles are practically identical or slightly lower to the changes of global irradiance (down to -2 W m^{-2} in CMIP5-D and down to -5 W m^{-2} in RCMs or CMIP6; see Fig. 5b). NetLW changes are small in all model ensembles and mostly insignificant (Fig. 5c). In RCMs, they tend to be year-round negative, the most in spring (down to -7 W m^{-2}). In all GCM families, NetLW changes are positive by a few watts per square meter from July to September, but not significantly. NetRAD changes closely follow the changes of NetSW, however, with a lower magnitude (Fig. 5d). NetRAD will increase in all GCM ensembles throughout the whole growing season (e.g., in CMIP5-D in absolute numbers up to $+17 \text{ W m}^{-2}$ in July, in relative numbers up to 13% in August). All changes are significant except for April. In RCMs, NetRAD will remain almost unchanged in

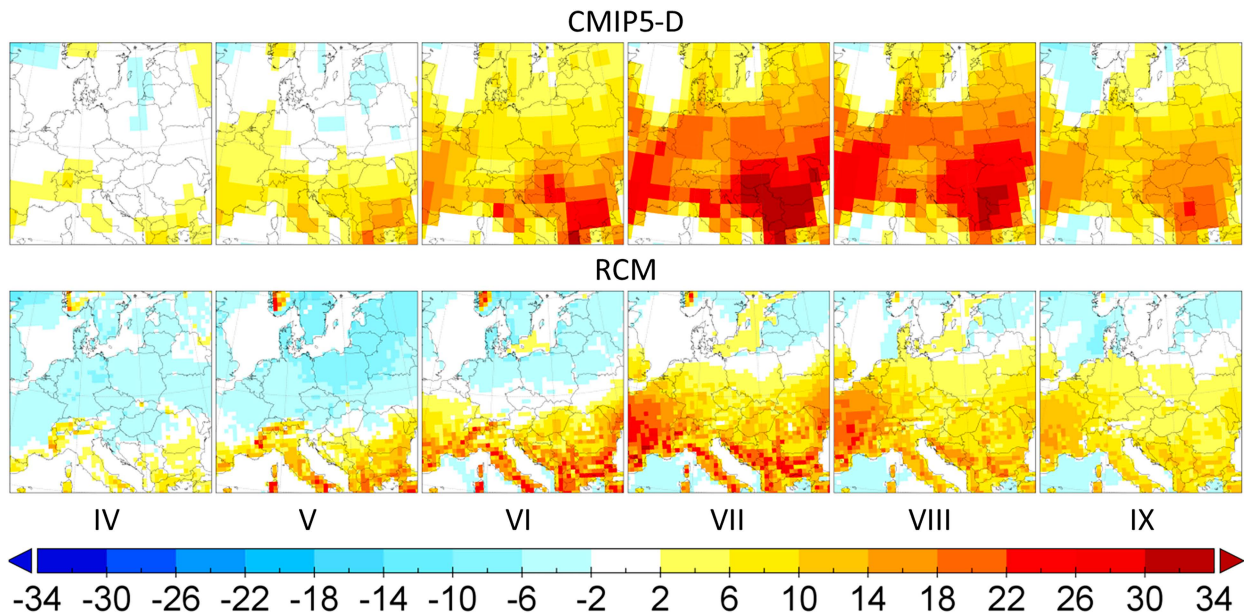
April and May. Then, NetRAD will rise, but positive changes are significant only in the second half of the growing season, and they always fall behind projected changes in CMIP5-D or other GCM ensembles (e.g., in July and August on -8 W m^{-2} compared to CMIP5-D).

The future growth of NetRAD in all models during the entire or part of the growing season will bring additional energy for Earth's surface compared to 1981–2005. This energy should be subsequently released in other nonradiative energy fluxes, for instance, via turbulent heat fluxes (H and LE).

5) LATENT HEAT FLUX

In all GCM ensembles, LE will increase from October to June (Fig. 5e), with maximal changes in spring months (e.g., CMIP5-D from $+7$ to $+8 \text{ W m}^{-2}$ or from $+10\%$ to $+22\%$). All GCM changes from October till May are significant. From July to September, LE will decrease slightly in GCMs (e.g., CMIP5-D -4 W m^{-2} or -6% in August), but changes are not significant in any of the GCM ensemble. Changes in LE are closely related to changes in precipitation (Fig. 4b). However, the relatively weak reduction in LE despite the strong decrease in precipitation in July or August suggests that LE evaporation (and thus evapotranspiration) is perhaps sustained at the expense of soil water storage in this period. The long-term balance between monthly precipitation and evapotranspiration results in negative values for the period May–August and reach cumulatively -85 mm which is about 30 mm more compared to 1981–2005.

In the RCMs, the monthly LE will increase only at a rate higher than or like that of the GCM ensembles (Fig. 5e). Even in the second part of the growing season, there is almost no grid point in central Europe where LE would drop less

FIG. 7. As in Fig. 6, but for H (W m^{-2}).

than -2 W m^{-2} (not shown) inferring on no pronounced long-term water limitations. The highest growth of LE is again expected to occur in spring with similar magnitude as that in the GCMs. Unlike GCMs, the increase of LE is also expected in June ($+7.9 \text{ W m}^{-2}$), and all positive changes from October till June are significant in RCMs. The changes in LE in the RCMs are again closely related to changes in precipitation. More precipitation (or a weaker reduction from July to September) together with stronger LE flux indicates that there will be a sufficient supply of soil moisture to enable evaporation. Compared to CMIP5-D, the long-term balance between monthly precipitation and evapotranspiration results in negative values only for the period June–August and reach cumulatively -37 mm (i.e., less than half of the water deficit in CMIP5-D) which is about 20 mm more than during 1981–2005.

6) SENSIBLE HEAT FLUX

According to all GCM ensembles, H will remain unchanged from November to April (Fig. 5f). From June to September, H will increase significantly, however. In July and August, the CMIP5-D projections suggest H up to $+19 \text{ W m}^{-2}$ (or $+50\%$) higher than in 1981–2005. While the changes in CMIP5 ensemble are like CMIP5-D, in CMIP6, they are stronger again, on additional $3\text{--}4 \text{ W m}^{-2}$. Higher values of H will affect only mainland Europe (Fig. 7). During the two-thirds of the central European growing season, H responds to the elevated global irradiance in all GCM ensembles at most and compensates for the higher income of energy through the absorption of shortwave solar radiation at the surface.

In the RCMs, the situation is different. In the spring, especially in April and May, the RCMs expect a reduction in H by -5 W m^{-2} (Fig. 5f). This reduction in H is limited to mainland Europe, approximately north of 47°N (Fig. 7). From July

to September, H will increase from $+3$ to $+6 \text{ W m}^{-2}$, but again, this rate is far behind the changes in the GCM ensembles that are 3 times stronger in magnitude (Fig. 5f). The amplification of H in the RCMs is the largest in the western part of central Europe and again limited to the mainland only (Fig. 7).

7) EVAPORATIVE FRACTION

Here, we strictly limit our investigation to the growing period, as the EF values may be distorted in late autumn, winter, and early spring, when both H and LE are small and additionally H is often negative. The EF changes are again different between RCMs on the one side and GCM ensembles on the other side.

In CMIP5-D as well as other GCM ensembles, the EF values will decrease except for April and May when they slightly rise or remain practically unchanged. From July to September, the EF will drop by -0.10 to -0.12 in CMIP5-D or by -0.12 to -0.17 in CMIP6 (Fig. 8). This is related to a tiny reduction in LE accompanied by a substantial increase in H and resulting changes of EF are significant across all GCM ensembles from July to September. In absolute terms from April to June, the EF values are practically identical to those in the past (i.e., approximately 0.7; see Fig. 3), while from July to September, they drop to 0.58 in CMIP5-D or 0.53 in CMIP6, reaching their minimum in August. The most significant declines in EF are in the water-limited southeastern and western Europe, where we also detect the most prominent changes in LE (reduction) and H (enhancement). This pattern is then also translated into geographical changes in EF in central Europe (Fig. 9).

In the RCMs, the EF rises from April to June (April $+0.07$, May $+0.05$; changes are significant) and then drops as in the GCMs but not as strongly (by -0.03 at most; see Fig. 8). The

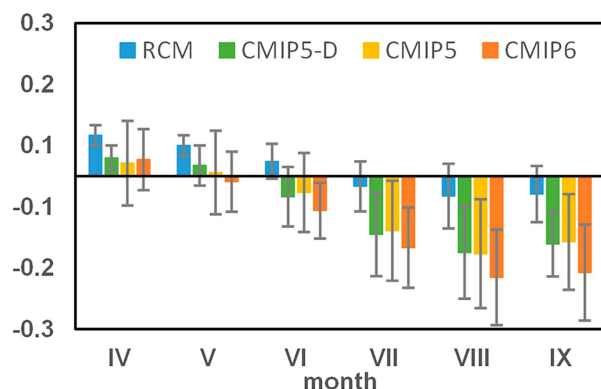


FIG. 8. Projected changes of the EF in central Europe in the last quarter of the twenty-first century according to the RCP8.5 scenario or SSP5-8.5 scenarios in EURO-CORDEX RCMs, their CMIP5-D, and other two larger ensembles of CMIP5 and CMIP6 GCMs. Whiskers indicate standard deviation of the ensemble mean changes.

role of LE on the net turbulent heat exchange is thus stronger and culminates at 0.81 in May. Then, it declines to 0.7 in July and August to rise again in September to 0.75 (not shown). The spring increase in the EF affects the whole of central Europe, while its summer reduction is particularly strong in the western part of central Europe (Fig. 9), where a combined effect of practically unchanged LE (not shown) and elevated H can be seen (Fig. 7).

4. Discussion and conclusions

We analyzed the surface energy budget of four ensembles of climate models and their future changes in the RCP8.5 or SSP5-8.5 scenario with emphasis on EURO-CORDEX RCMs

and their driving CMIP5 GCMs. When RCMs and CMIP5-D are tested in central Europe against the gridded observational datasets represented by ERA5-Land, E-OBS, and SARAH-2, a surprisingly excellent agreement in the simulated LE in terms of mean bias was found in all months of the growing season in the period of 1981–2005. This suggests that evapotranspiration, a key component of the water cycle, and energy or mass exchange between the land surface and atmosphere, is well, or at least consistently, captured in terms of the size in the recent generation of climate models in central Europe, even though the spatial distribution of LE does not show good agreement with ERA5-Land.

The evaluation also reveals the existence of important biases in other fluxes, especially in CMIP5-D. There is a significant overestimation of global irradiance in CMIP5-D that further propagates into other energy fluxes: NetSW, NetLW, and H (Fig. 2). As noted by Wild (2020), excessive global irradiance is related to a lack of absorption in the cloud-free atmosphere in the GCMs and persists even in the latest generation of CMIP6 GCMs. It is then translated into increased NetLW and H , leading to their biases when compared to ERA5-Land.

Overall, very good agreement between the RCMs and ERA5-Land was found. In some cases, the spatial distribution of energy fluxes and their seasonal courses seem to be even more realistic in the RCMs than in ERA5-Land. First, the spatial distribution of global irradiance is rather smoothed in ERA5-Land (or E-OBS), while in RCMs or CM SAF satellite observation, it is more detailed and captures, for instance, a summer reduction of global irradiance over the mountains (Fig. A1 in the appendix). Second, the stronger role of H in RCMs detected in central Europe (Fig. 5f) and its lowlands in summer (Fig. A2 in the appendix) corresponds well to the behavior of typical lowland biomes, e.g., crop fields, as confirmed by FLUXNET measurements (Fig. A3 in the appendix). An

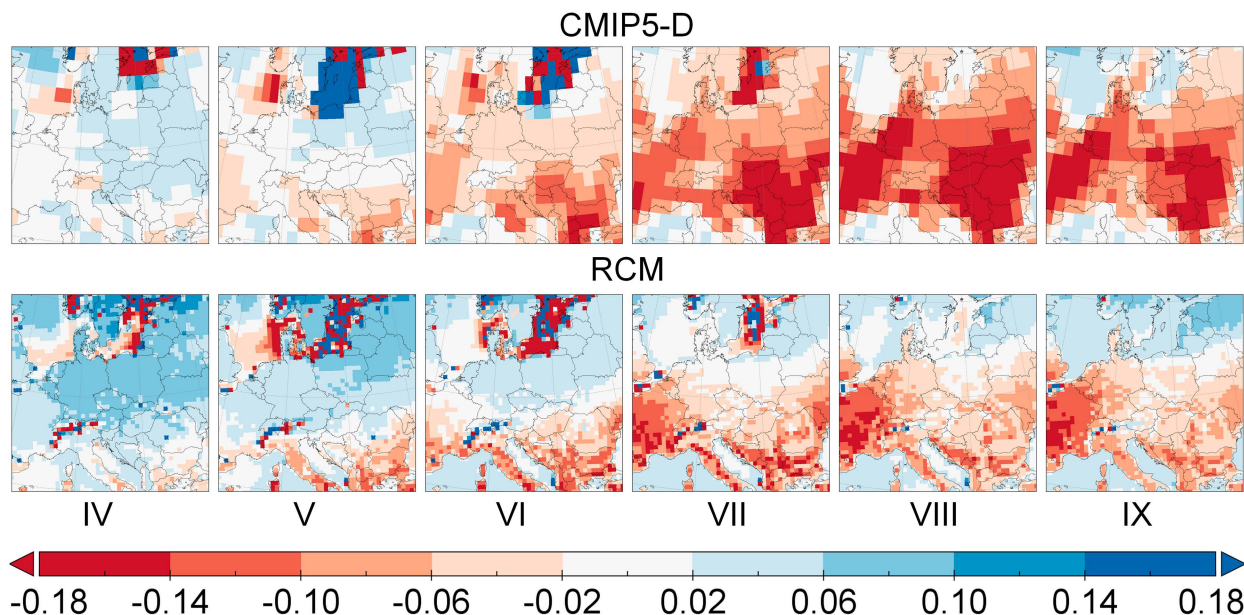


FIG. 9. As in Fig. 6, but for the EF.

intensification of H in RCMs is also accompanied by a reduction in LE in the summer months (Fig. A2 in the appendix). ERA5-Land, however, keeps H constant throughout almost the entire growing season (Fig. 2f). Similar behavior is typical for grassland, as indicated by FLUXNET measurements (Fig. A3 in the appendix). However, this is not a dominant biome of central Europe. According to the Coordination of Information on the Environment (CORINE2020), it represents only 10% of the land surface of central Europe. The practically constant seasonal course of H in the growing season in ERA5-Land could be explained because of spatial averaging over the study area, where a mixture of forests (32%), crop fields (44%), or pastures (10%) is present. As illustrated by the measurements at FLUXNET sites, these major central European biomes show very diverse seasonal courses of H and also EF (Fig. A3 in the appendix). However, even at finer spatial scales in ERA5-Land, for instance, over the large agricultural lowlands of Slovakia, Hungary, or Central Bohemia, there is no sign of temporal variability of H that is typical for FLUXNET cropland sites. With respect to the high resolution of ERA5-Land (0.1°) and its maternal ERA5 reanalysis (0.25°), it is surprising. Both examples point on the added value of RCMs as a tool for downscaling global climate models and simulating climate on a regional or local scale.

Future changes in all investigated surface energy budget components are mainly affected and driven by changes in global irradiance and the net balance of shortwave radiation. This is where we see an important difference between GCM and RCM simulations, as noted by Bartók et al. (2017) and more closely investigated by Boé et al. (2020) or Taranu et al. (2023).

In all GCM ensembles, we see an increase in global irradiance for most of the year that is translated into a year-round enhancement of NetSW. It is then balanced mostly by higher turbulent heat fluxes. In the first 2 months of the growing season in central Europe, we see the abundance of water from precipitation in winter and spring that is translated into a higher LE flux and, despite higher temperatures, a constant H . From June to September, the rainfall drops, followed by an immediate increase in H and a subsequent small reduction in LE. Evapotranspiration is likely limited by the soil water supply. The second part of the growing season is warm, sunny, and dry. All GCM projections thus indicate higher likelihood of conditions that may cause drought stress to vegetation due to lack of water and overall decrease in biomass productivity, despite higher CO_2 levels.

The situation is less straightforward in the RCMs, where changes in global irradiance and NetSW are balanced differently. There is a reduction in NetLW throughout the year. With respect to rising air temperatures and elevated concentrations of greenhouse gases in the atmosphere, the reduction in NetLW can be explained by the strengthening of downwelling longwave radiation. This is likely due to greater cloudiness, as also indicated by the reduction in global irradiance. The LE flux is enhanced throughout the year, most strongly in spring and early summer, which is again related to high precipitation and warmer climate in winter and spring. Evapotranspiration does not seem to be limited by the soil water supply, as also indicated by the reduced H and simple

water balance consideration leading relatively small summer deficits. From July to September, the temperature rises, the rainfall drops, the sky becomes brighter, and Earth's surface gains more energy, but it is still far less than that in the CMIP5-D. Evapotranspiration is still slightly higher than at present, and compared to H , LE dominates in compensating the small energy gains due to the higher NetSW. The second part of the growing season is warm and sunny but certainly not dry. All this happens under high concentrations of CO_2 . The RCM scenarios thus indicate conditions that are favorable for a substantial increase in plant productivity due to the abundance of water or the overall prolonging of the growing season.

Although the detected differences between CMIP5-D and RCM projections in central Europe seem to be insignificant, their combination can have fundamental effects on the estimation of the very nature of the impact of climate change on some sectors. The predictions of the impact models can lead to remarkably different results, which cannot be explained simply by reference to the different resolution or uncertainty in the CMIP5-D and RCM ensembles.

Furthermore, when the wider ensemble consisted of 17 CMIP6 GCMs and their projections following the shared socio-economic pathway (SSP) scenario SSP5-85 is considered, differences between the CMIP5-D or CMIP5 and RCM projections become even more pronounced. Although the SSP5-85 and RCP8.5 scenarios are not identical and the new generation CMIP6 models show greater climate sensitivity than their CMIP5 counterparts (Meehl et al. 2020; Zelinka et al. 2020), the overall pattern of the future changes of air temperature, precipitation, and surface energy budget components in the CMIP6 ensemble is closer to both CMIP5 ensembles and further away from RCMs (Fig. 5). Warming is generally stronger in CMIP6 and associated with a more significant reduction of precipitation in the growing season. The global irradiance increase is also stronger, especially from April to June. LE and H changes in CMIP6 follow a similar pattern as in CMIP5 ensembles, but again, the magnitude of change is bigger. Their combined effect leads to larger reduction of EF in the growing season. There is no sign of heading toward the wetter growing season in central Europe.

It is also worth noting that the observed data in central Europe show the following:

- 1) increase in global irradiance in the first half of the growing season (Trnka et al. 2015),
- 2) long-term stagnation of annual precipitation (Brázdil et al. 2022),
- 3) prolongation of drought episodes (Trnka et al. 2016),
- 4) reduction of water supply in the soil (Trnka et al. 2015, 2022; Scherrer et al. 2022),
- 5) decrease in river discharge (Fischer et al. 2023; Torbenson et al. 2023), and
- 6) reduction of underground water supply (Hellwig and Stahl 2018).

All of the abovementioned phenomena are compatible with the GCM projections of the central European climate in the twenty-first century. On the other hand, climate conditions

projected by RCMs in central Europe have a significantly weaker fingerprint in observations thus far, although the signal of human-induced global climate change has already been present in observations for many decades. EURO-CORDEX RCM simulations obtained by downscaling CMIP5-D result in changes in global irradiance, turbulent heat fluxes, or precipitation that lead to conditions favorable for landscape water accumulation and plant growth in the growing season in central Europe. This is, however, in contradiction with the story told by CMIP5-D and trends derived from observations. Although the added value of RCMs and their suitability for use in impact studies is evident, in the case of the conflicting nature of RCM and GCM projections, the emphasis on using RCM-based projections in further modeling and decision-making chains might lead to a serious risk of maladaptation and inefficiencies in mitigating climate change.

Our results thus confirm the ongoing need for more detailed investigation and better understanding of causes that lead to differences among climate projections from different model ensembles, as they have already been initiated by the climate modeling community (Fernández et al. 2019; Schwingshackl et al. 2019; Boé et al. 2020; Taranu et al. 2023). It is worth noting that in EURO-CORDEX experiments downscaling CMIP5 models in higher spatial resolution of 0.11°, there are RCMs with evolving aerosols and thus different evolution of air temperature or global irradiance (Schumacher et al. 2024). Our results for EURO-CORDEX 0.44° RCMs do not comprise the full available CORDEX RCM ensemble. For future use of RCMs, we suggest introducing the preliminary test of RCMs by using their data in impact models to critically examine a cumulative effect of potential biases that may be hidden in RCMs. Comparing these outputs with the observations may serve as an indirect validation of RCMs prior to their recommendation as a tool for impact studies. In light of the arrival of a new generation of EURO-CORDEX projections based on the downscaling of CMIP6 GCMs, this is a timely note that may help to support and confirm the choice

of the most suitable RCMs for impact modeling in all parts of Europe.

Acknowledgments. This study was supported by the project “AdAgriF—advanced methods of greenhouse gases emission reduction and sequestration in agriculture and forest landscape for climate change mitigation” (CZ.02.01.01/00/22_008/0004635). M. Fischer and M. Hlavsová were supported by Czech Science Foundation Grant 24-12935S. We acknowledge providers and producers of all climate model and observational data used in this study. Our special thanks go to the principal investigators of FLUXNET sites for their kind permission to use their data for illustration purposes in our work.

Data availability statement. GCM and RCM data are available via the ESGF data nodes (see, e.g., <https://esgf.llnl.gov/nodes.html>). ERA5-Land and E-OBS data are available via Climate Data Store of Copernicus Climate Change Services (<https://cds.climate.copernicus.eu#!/home>). SARAH-2 data were obtained via the web user interface at the CM SAF (https://wui.cmsaf.eu/safira/action/viewHome?menuName=HOME_CMSAF_WUI). FLUXNET station data were collected by Alexander Graf from managers of individual FLUXNET sites.

APPENDIX

FLUXNET Stations and Evaluation of RCMs and CMIP5-D GCMs

We used measurements of surface energy balance components from selected stations of the FLUXNET network in central Europe to illustrate surface turbulent heat fluxes behavior in different biomes typical for central Europe and to compare with climate model data. The data from FLUXNET sites cover the period 2001–18; however, availability may differ among stations (Table A1). Additional details are provided in Figs. A1–A3.

TABLE A1. Availability of radiation and heat flux data from the selected FLUXNET stations representing various biomes in central Europe.

Map ID	Biome	Site	Alt	Lon	Lat	Data coverage	Reference
A	Crop	Oensing	452	7.734	47.286	2004–18	Emmel et al. (2018)
B	Grass	Chamau	400	8.410	47.210	2006–18	Feigenwinter et al. (2023)
C	Forest	Hainich	440	10.453	51.079	2001–18	Knohl et al. (2003)
D	Crop	Gebesee	162	10.914	51.100	2001–18	
E	Crop	Klingenberg	478	13.522	50.893	2005–18	Prescher et al. (2010)
F	Grass	Grillenburg	385	13.513	50.950	2003–18	Prescher et al. (2010)
G	Forest	Tharandt	380	13.565	50.963	2001–18	Prescher et al. (2010)
H	Forest	Bílý Kříž	875	18.537	49.502	2004–18	

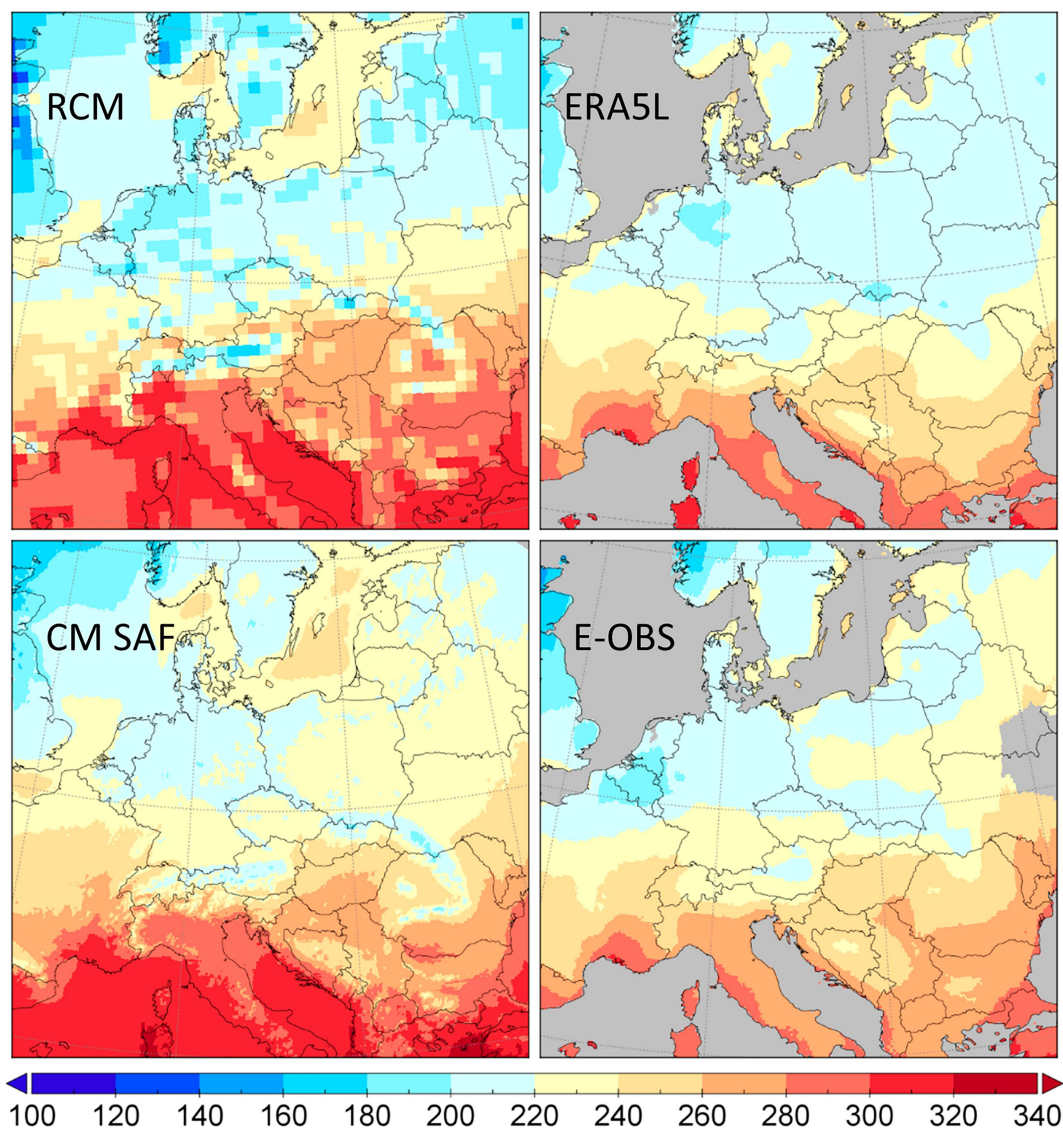


FIG. A1. (clockwise from the top-left corner) Monthly mean global irradiance (W m^{-2}) in July derived from EURO-CORDEX RCMs, ERA5-Land, E-OBS, and CM SAF SARAH-2 data in the period 1981–2005.

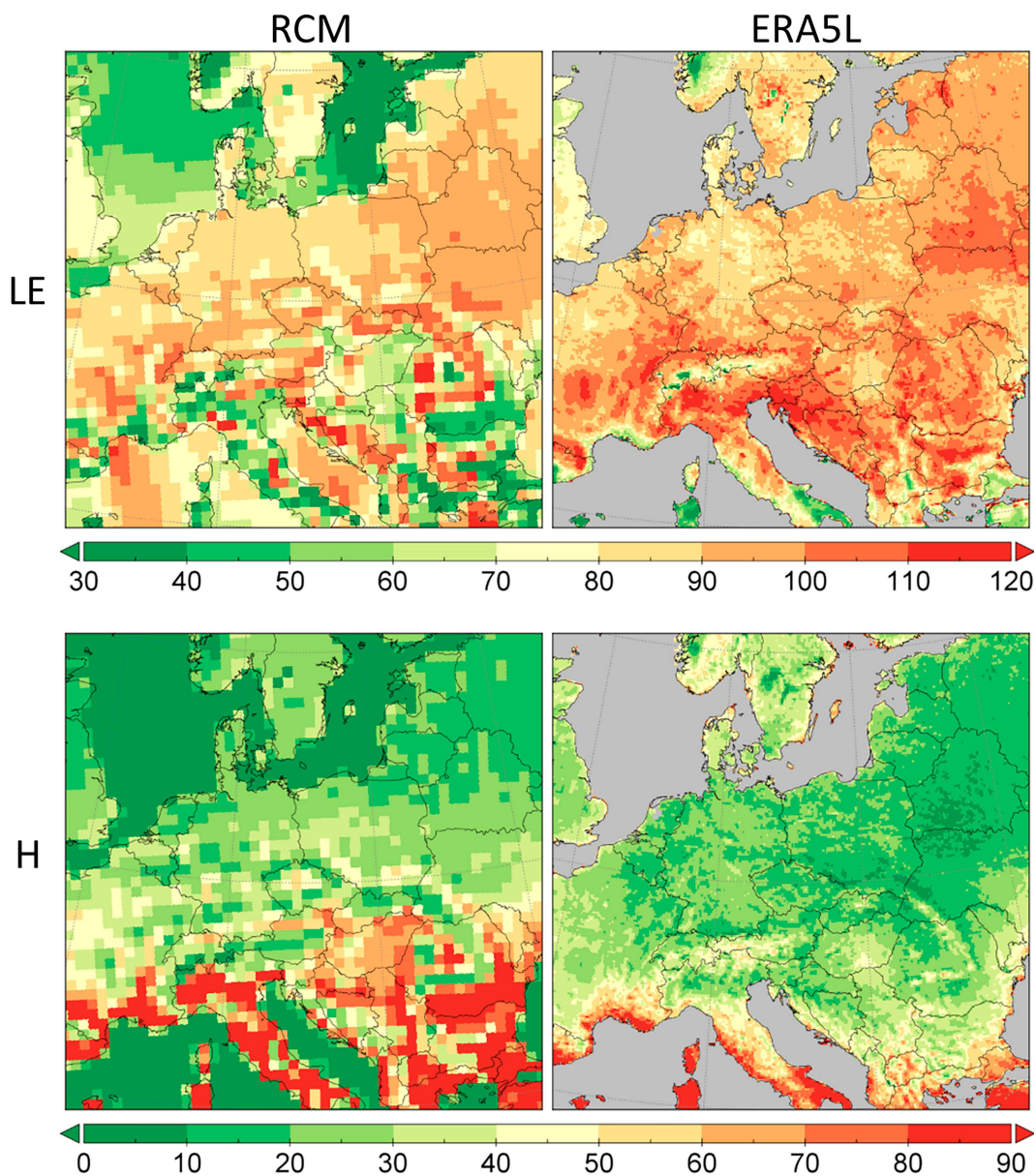


FIG. A2. (top) Monthly mean latent and (bottom) sensible heat flux (W m^{-2}) in July derived from (left) EURO-CORDEX RCM and (right) ERA5L in the period 1981–2005.

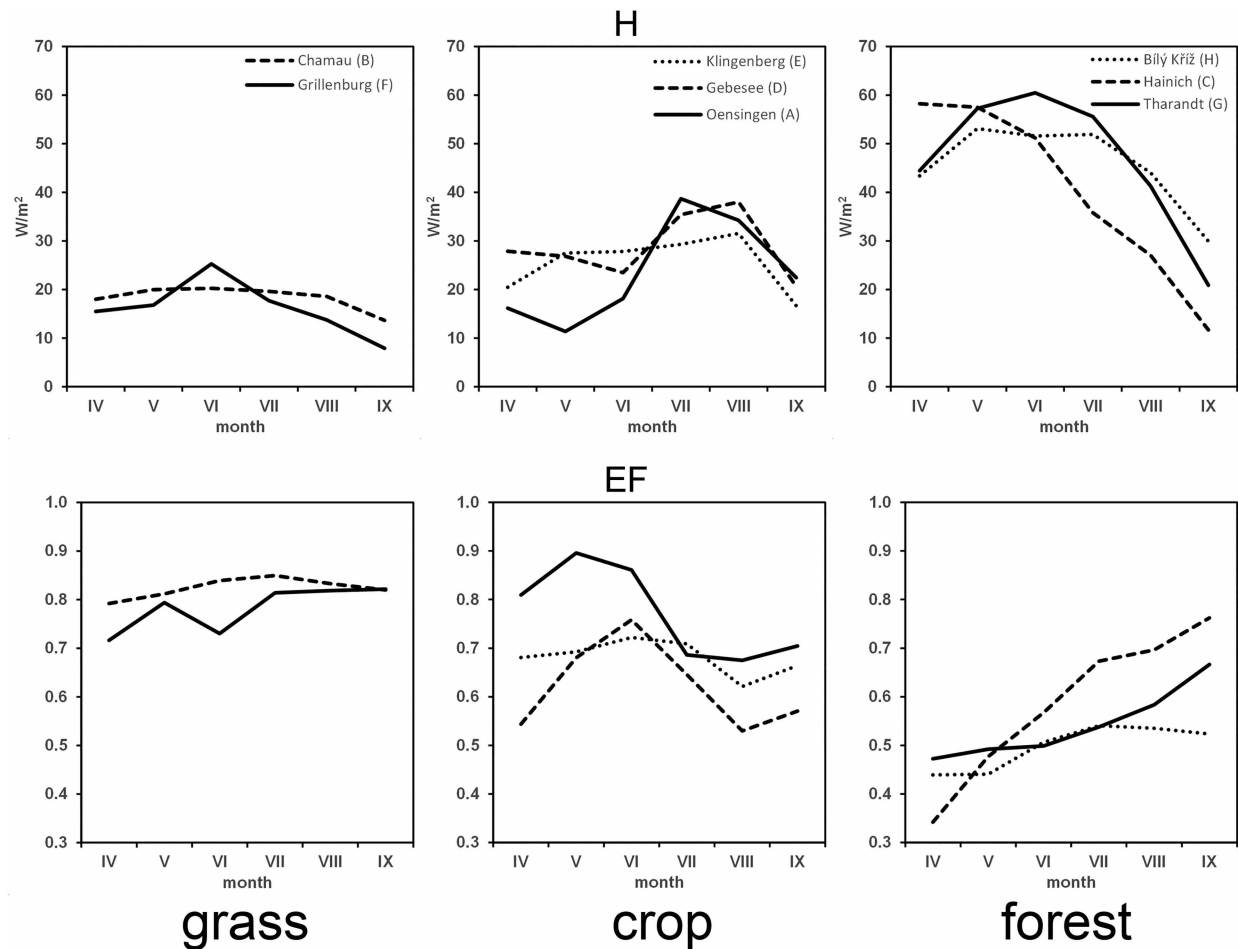


FIG. A3. Seasonal course of (top) H (W m^{-2}) and (bottom) the EF from April (IV) to September (IX) at selected central European FLUXNET sites representing various biomes: (left) grassland, (center) cropland, and (right) forest.

REFERENCES

- Bartók, B., and Coauthors, 2017: Projected changes in surface solar radiation in CMIP5 global climate models and in EURO-CORDEX regional climate models for Europe. *Climate Dyn.*, **49**, 2665–2683, <https://doi.org/10.1007/s00382-016-3471-2>.
- Boé, J., S. Somot, L. Corre, and P. Nabat, 2020: Large discrepancies in summer climate change over Europe as projected by global and regional climate models: Causes and consequences. *Climate Dyn.*, **54**, 2981–3002, <https://doi.org/10.1007/s00382-020-05153-1>.
- Brázdil, R., P. Zahradníček, P. Dobrovolný, J. Řehoř, M. Trnka, O. Lhotka, and P. Štěpánek, 2022: Circulation and climate variability in the Czech Republic between 1961 and 2020: A comparison of changes for two “normal” periods. *Atmosphere*, **13**, 137, <https://doi.org/10.3390/atmos13010137>.
- Coppola, E., and Coauthors, 2021: Assessment of the European climate projections as simulated by the large EURO-CORDEX regional and global climate model ensemble. *J. Geophys. Res. Atmos.*, **126**, e2019JD032356, <https://doi.org/10.1029/2019JD032356>.
- Cornes, R. C., G. van der Schrier, E. J. M. van den Besselaar, and P. D. Jones, 2018: An ensemble version of the E-OBS temperature and precipitation data sets. *J. Geophys. Res. Atmos.*, **123**, 9391–9409, <https://doi.org/10.1029/2017JD028200>.
- Emmel, C., A. Winkler, L. Hörtnagl, A. Revill, C. Ammann, P. D’Odorico, N. Buchmann, and W. Eugster, 2018: Integrated management of a Swiss cropland is not sufficient to preserve its soil carbon pool in the long term. *Biogeosciences*, **15**, 5377–5393, <https://doi.org/10.5194/bg-15-5377-2018>.
- Enriquez-Alonso, A., J. Calbó, A. Sanchez-Lorenzo, and E. Tan, 2017: Discrepancies in the climatology and trends of cloud cover in global and regional climate models for the Mediterranean region. *J. Geophys. Res. Atmos.*, **122**, 11 644–11 677, <https://doi.org/10.1002/2017JD027147>.
- Eyring, V., S. Bony, G. A. Meehl, C. A. Senior, B. Stevens, R. J. Stouffer, and K. E. Taylor, 2016: Overview of the Coupled Model Intercomparison Project Phase 6 (CMIP6) experimental design and organization. *Geosci. Model Dev.*, **9**, 1937–1958, <https://doi.org/10.5194/gmd-9-1937-2016>.
- Feigenwinter, I., L. Hörtnagl, M. J. Zeeman, W. Eugster, K. Fuchs, L. Merbold, and N. Buchmann, 2023: Large interannual variation in carbon sink strength of a permanent grassland over 16 years: Impacts of management practices and

- climate. *Agric. For. Meteorol.*, **340**, 109613, <https://doi.org/10.1016/j.agrformet.2023.109613>.
- Fernández, J., and Coauthors, 2019: Consistency of climate change projections from multiple global and regional model inter-comparison projects. *Climate Dyn.*, **52**, 1139–1156, <https://doi.org/10.1007/s00382-018-4181-8>.
- Fischer, M., and Coauthors, 2023: Attributing the drivers of runoff decline in the Thaya river basin. *J. Hydrol.*, **48**, 101436, <https://doi.org/10.1016/j.ejrh.2023.101436>.
- Giorgi, F., 2019: Thirty years of regional climate modeling: Where are we and where are we going next? *J. Geophys. Res. Atmos.*, **124**, 5696–5723, <https://doi.org/10.1029/2018JD030094>.
- , C. Jones, and G. R. Asrar, 2009: Addressing climate information needs at the regional level: The CORDEX framework. *WMO Bull.*, **58**, 175–183.
- Gutiérrez, J. M., and Coauthors, 2023: Atlas. *Climate Change 2021: The Physical Science Basis*, V. Masson-Delmotte et al., Eds., Cambridge University Press, 1927–2058, <https://doi.org/10.1017/9781009157896.021>.
- Hellwig, J., and K. Stahl, 2018: An assessment of trends and potential future changes in groundwater-baseflow drought based on catchment response times. *Hydrol. Earth Syst. Sci.*, **22**, 6209–6224, <https://doi.org/10.5194/hess-22-6209-2018>.
- Hersbach, H., and Coauthors, 2017: The ERA5 global reanalysis. *Quart. J. Roy. Meteor. Soc.*, **146**, 1999–2049, <https://doi.org/10.1002/qj.3803>.
- IPCC, 2021: *Climate Change 2021: The Physical Science Basis*. Cambridge University Press, 2392 pp., <https://doi.org/10.1017/9781009157896>.
- Katul, G. G., R. Oren, S. Manzoni, C. Higgins, and M. B. Parlange, 2012: Evapotranspiration: A process driving mass transport and energy exchange in the soil-plant-atmosphere-climate system. *Rev. Geophys.*, **50**, RG3002, <https://doi.org/10.1029/2011RG000366>.
- Kendon, E. J., A. F. Prein, C. A. Senior, and A. Stirling, 2021: Challenges and outlook for convection-permitting climate modelling. *Philos. Trans. Roy. Soc.*, **A379**, 20190547, <https://doi.org/10.1098/rsta.2019.0547>.
- Knist, S., and Coauthors, 2017: Land-atmosphere coupling in EURO-CORDEX evaluation experiments. *J. Geophys. Res. Atmos.*, **122**, 79–103, <https://doi.org/10.1002/2016JD025476>.
- Knohl, A., E.-D. Schulze, O. Kolle, and N. Buchmann, 2003: Large carbon uptake by an unmanaged 250-year-old deciduous forest in Central Germany. *Agric. For. Meteorol.*, **118**, 151–167, [https://doi.org/10.1016/S0168-1923\(03\)00115-1](https://doi.org/10.1016/S0168-1923(03)00115-1).
- Lucas-Picher, P., D. Argüeso, E. Brisson, Y. Trambay, P. Berg, A. Lemonsu, S. Kotlarski, and C. Caillaud, 2021: Convection-permitting modeling with regional climate models: Latest developments and next steps. *Wiley Interdiscip. Rev.: Climate Change*, **12**, e731, <https://doi.org/10.1002/wcc.731>.
- Meehl, G. A., C. A. Senior, V. Eyring, G. Flato, J.-F. Lamarque, R. J. Stouffer, K. E. Taylor, and M. Schlund, 2020: Context for interpreting equilibrium climate sensitivity and transient climate response from the CMIP6 Earth system models. *Sci. Adv.*, **6**, eaba1981, <https://doi.org/10.1126/sciadv.aba1981>.
- Muñoz-Sabater, J., and Coauthors, 2021: ERA5-Land: A state-of-the-art global reanalysis dataset for land applications. *Earth Syst. Sci. Data*, **13**, 4349–4383, <https://doi.org/10.5194/essd-13-4349-2021>.
- Nabat, P., S. Somot, M. Mallet, A. Sanchez-Lorenzo, and M. Wild, 2014: Contribution of anthropogenic sulfate aerosols to the changing Euro-Mediterranean climate since 1980. *Geophys. Res. Lett.*, **41**, 5605–5611, <https://doi.org/10.1002/2014GL060798>.
- O'Neill, B. C., and Coauthors, 2016: The Scenario Model Inter-comparison Project (ScenarioMIP) for CMIP6. *Geosci. Model Dev.*, **9**, 3461–3482, <https://doi.org/10.5194/gmd-9-3461-2016>.
- Pfieferth, U., S. Kothe, J. Trentmann, R. Hollmann, P. Fuchs, J. Kaiser, and M. Werscheck, 2019: Surface radiation data set - Heliosat (SARAH) - edition 2.1. Satellite Application Facility on Climate Monitoring, https://doi.org/10.5676/EUM_SAF_CM/SARAH/V002_01.
- Prein, A. F., R. Rasmussen, and G. Stephens, 2017: Challenges and advances in convection-permitting climate modeling. *Bull. Amer. Meteor. Soc.*, **98**, 1027–1030, <https://doi.org/10.1175/BAMS-D-16-0263.1>.
- Prescher, A.-K., T. Grünwald, and C. Bernhofer, 2010: Land use regulates carbon budgets in eastern Germany: From NEE to NBP. *Agric. For. Meteorol.*, **150**, 1016–1025, <https://doi.org/10.1016/j.agrformet.2010.03.008>.
- Scherrer, S. C., M. Hirschi, C. Spirig, F. Maurer, and S. Kotlarski, 2022: Trends and drivers of recent summer drying in Switzerland. *Environ. Res. Commun.*, **4**, 025004, <https://doi.org/10.1088/2515-7620/ac4fb9>.
- Schumacher, D. L., J. Singh, M. Hauser, E. Fischer, and S. Seneviratne, 2024: Exacerbated summer European warming not captured by climate models neglecting long-term aerosol changes. *Commun., Earth Environ.*, **5**, 182, <https://doi.org/10.1038/s43247-024-01332-8>.
- Schwingshackl, C., E. L. Davin, M. Hirschi, S. L. Sørland, R. Wartenburger, and S. I. Seneviratne, 2019: Regional climate model projections underestimate future warming due to missing plant physiological CO₂ response. *Environ. Res. Lett.*, **14**, 114019, <https://doi.org/10.1088/1748-9326/ab4949>.
- Sørland, S. L., C. Schär, D. Lühti, and E. Kjellström, 2018: Bias patterns and climate change signals in GCM-RCM model chains. *Environ. Res. Lett.*, **13**, 074017, <https://doi.org/10.1088/1748-9326/aacc77>.
- Stagehuis, A. I., R. Vautard, P. Ciais, A. J. Teuling, M. Jung, and P. You, 2013: Summer temperatures in Europe and land heat fluxes in observation-based data and regional climate model simulations. *Climate Dyn.*, **41**, 455–477, <https://doi.org/10.1007/s00382-012-1559-x>.
- Taranu, I. S., S. Somot, A. Alias, J. Boé, and C. Delire, 2023: Mechanisms behind large-scale inconsistencies between regional and global climate model-based projections over Europe. *Climate Dyn.*, **60**, 3813–3838, <https://doi.org/10.1007/s00382-022-06540-6>.
- Taylor, K. E., R. J. Stouffer, and G. A. Meehl, 2012: An overview of CMIP5 and the experiment design. *Bull. Amer. Meteor. Soc.*, **93**, 485–498, <https://doi.org/10.1175/BAMS-D-11-00094.1>.
- Torbenson, M. C. A., and Coauthors, 2023: Increasing volatility of reconstructed Morava River warm-season flow, Czech Republic. *J. Hydrol.*, **50**, 101534, <https://doi.org/10.1016/j.ejrh.2023.101534>.
- Trnka, M., and Coauthors, 2015: Drivers of soil drying in the Czech Republic between 1961 and 2012. *Int. J. Climatol.*, **35**, 2664–2675, <https://doi.org/10.1002/joc.4167>.
- , and Coauthors, 2016: Drought trends over part of Central Europe between 1961 and 2014. *Climate Res.*, **70**, 143–160, <https://doi.org/10.3354/cr01420>.
- , and Coauthors, 2022: Increasing available water capacity as a factor for increasing drought resilience or potential conflict

- over water resources under present and future climate conditions. *Agric. Water Manage.*, **264**, 107460, <https://doi.org/10.1016/j.agwat.2022.107460>.
- Wilby, R. L., and T. M. L. Wigley, 1997: Downscaling general circulation model output: A review of methods and limitations. *Prog. Phys. Geogr.*, **21**, 530–548, <https://doi.org/10.1177/030913339702100403>.
- Wild, M., 2020: The global energy balance as represented in CMIP6 climate models. *Climate Dyn.*, **55**, 553–577, <https://doi.org/10.1007/s00382-020-05282-7>.
- Zelinka, M. D., T. A. Myers, D. T. McCoy, S. Po-Chedley, P. M. Caldwell, P. Ceppi, S. A. Klein, and K. E. Taylor, 2020: Causes of higher climate sensitivity in CMIP6 models. *Geophys. Res. Lett.*, **47**, e2019GL085782, <https://doi.org/10.1029/2019GL085782>.